Multi-species ITG-TEM driven turbulent transport of D-T ions and He-ash in ITER burning plasmas

M. Nakata[1,2], M. Honda[3], M. Nunami[1,2], T. -H. Watanabe[4] and H. Sugama[1,2]

[1]National Institute for Fusion Science/National Institutes of Natural Sciences, Toki, Japan
[2]Graduate University for Advanced Studies, Toki, Japan
[3]National Institutes for Quantum and Radiological Science and Technology, Naka, Japan
[4]Department of Physics, Nagoya University, Nagoya, Japan

Corresponding Author: nakata.motoki@nifs.ac.jp

Abstract:
Ion temperature gradient and trapped electron modes (ITG-TEM) driven turbulent transport in realistic ITER plasmas is investigated by means of multi-species electromagnetic gyrokinetic Vlasov simulations with D, T, He, and real-mass kinetic electrons including their inter-species collisions. A good prediction capability of the local gyrokinetic simulation has been confirmed against the JT-60U tokamak L-mode experiment. For the ITER D-T-He plasma, gyrokinetic-simulation-based quantitative evaluation of a steady burning condition with He-ash exhaust and fuel inward-pinch is realized by extensive nonlinear scans. Furthermore, the strong impacts of D-T fuel ratio and He-ash accumulations on turbulent energy and particle fluxes are clarified. New findings in this study, which are crucial for the burning plasma performance, are (i)imbalanced D-T turbulent particle transport strongly influenced by He-ash accumulations, and (ii)identification of the steady burning profile regimes with He-ash exhaust and D-T fuel inward-pinch associated with the off-diagonal transport.

1 Introduction

The first-principle based gyrokinetic simulation is widely recognized as a promising way to predict turbulent transport driven by microinstabilities such as ion temperature gradient(ITG) modes, trapped electron modes(TEM), and electron temperature gradient(ETG) modes in magnetically confined fusion plasmas. Nowadays the validation studies against existing experiments also become more active[1, 2, 3, 4]. However, turbulent transport properties in multiple ion species plasmas, including hydrogen isotope and impurity effects, have not been fully clarified. Actually, burning plasmas are always composed of multi-ion species such as fuel isotopes (Deuterium and Tritium) and He-ash produced by the fusion reaction, and more complex turbulent transport processes are expected in comparison to the single-ion-species plasmas. Since simultaneous measurements of the kinetic profiles for all species are limited in experiments, systematic studies on the particle

and heat transport are indispensable to predict the confinement performance and to optimize the impurity exhausts and D/T fueling. There are several earlier works regarding the ITG driven turbulent transport of D-T fuel ions[5, 6] and the light and heavy impurity transport[7, 8], but the fuel and impurity ion transport has been examined separately.

In this study, the ITG-TEM driven turbulent transport in realistic ITER plasmas is investigated by means of the gyrokinetic Vlasov simulation GKV[9, 10] with D, T, He, and real-mass kinetic electrons including their inter-species collisions[11], where a good prediction capability of the code has been confirmed against the JT-60U tokamak L-mode experiment[4]. In addition to the D-T fuel ratio and He-ash accumulation dependence of the turbulent transport levels, the simultaneous treatment of D-T and He-ash ions enables us to explore the optimum profiles regimes, which satisfy a steady burning condition[12] with He-ash exhaust and fuel inward-pinch.

2 Multi-species gyrokinetic simulation model with realistic tokamak equilibrium

2.1 Calculation model

Calculation model used in GKV is briefly summarized in this section. The governing equation is an electromagnetic gyrokinetic Vlasov equation for arbitrary particle species, which describes the time evolution of $\delta g_{\rm s}$ ("s" is the index of particle species), i.e., the non-adiabatic part of the perturbed gyrocenter distribution function $\delta f_{\rm s}^{\rm (g)}$ on the five-dimensional phase-space $(\boldsymbol{x}_{\rm g}, v_\parallel, \mu)$. The Fourier representation with respect to the perpendicular wavenumber $\boldsymbol{k}_\perp$ is given by

$$\left(\frac{\partial}{\partial t} + v_\parallel \boldsymbol{b}\cdot\nabla + i\omega_{\rm Ds} - \frac{\mu \boldsymbol{b}\cdot\nabla B}{m_{\rm s}}\frac{\partial}{\partial v_\parallel}\right)\delta g_{{\rm s}\boldsymbol{k}_\perp} - \frac{c}{B}\sum_{\Delta} \boldsymbol{b}\cdot(\boldsymbol{k}'_\perp \times \boldsymbol{k}''_\perp)\,\delta\psi_{{\rm s}\boldsymbol{k}'_\perp}\delta g_{{\rm s}\boldsymbol{k}''_\perp}$$
$$= \frac{e_{\rm s}F_{\rm Ms}}{T_{\rm s}}\left(\frac{\partial}{\partial t} + i\omega_{*T{\rm s}}\right)\delta\psi_{{\rm s}\boldsymbol{k}_\perp} + \mathcal{C}_{\rm s}(\delta g_{{\rm s}\boldsymbol{k}_\perp}) \ , \qquad (1)$$

where $\delta g_{{\rm s}\boldsymbol{k}_\perp} = \delta f^{\rm (g)}_{{\rm s}\boldsymbol{k}_\perp} + F_{\rm Ms}J_{0{\rm s}}e_{\rm s}\delta\phi_{\boldsymbol{k}_\perp}/T_{\rm s}$, and $J_{0{\rm s}} = J_0(k_\perp v_\perp/\Omega_{\rm s})$ is the zeroth-order Bessel function. The gyrophase-averaged electrostatic and electromagnetic potential fluctuations are combined into $\delta\psi_{{\rm s}\boldsymbol{k}_\perp} = J_{0{\rm s}}\delta\phi_{\boldsymbol{k}_\perp} - (v_\parallel/c)J_{0{\rm s}}\delta A_{\parallel\boldsymbol{k}_\perp}$. Since we focus on the finite but low-β plasmas here, the parallel magnetic field fluctuation $\delta B_{\parallel\boldsymbol{k}_\perp}$ is ignored. The equilibrium part of the distribution function is given by the local Maxwellian distribution, i.e., $F_{\rm Ms} = n_{\rm s}(m_{\rm s}/2\pi T_{\rm s})^{3/2}\exp[-(m_{\rm s}v_\parallel^2 + 2\mu B)/2T_{\rm s}]$. Collisional effects are introduced in terms of a multi-species gyrokinetic collision operator $\mathcal{C}_{\rm s}$ expressed as

$$\mathcal{C}_{\rm s}(\delta g_{{\rm s}\boldsymbol{k}_\perp}) = \sum_{\rm s'}\oint\frac{d\varphi}{2\pi}e^{i\boldsymbol{k}_\perp\cdot\boldsymbol{\rho}_{\rm s}}\left\{\mathcal{C}^{\rm T}_{\rm ss'}[e^{-i\boldsymbol{k}_\perp\cdot\boldsymbol{\rho}_{\rm s}}\delta g_{{\rm sk}_\perp}] + \mathcal{C}^{\rm F}_{\rm ss'}[e^{-i\boldsymbol{k}_\perp\cdot\boldsymbol{\rho}_{\rm s'}}\delta g_{{\rm s'k}_\perp}]\right\} \qquad (2)$$

where the field-particle part $\mathcal{C}^{\rm F}_{\rm ss'}$ holds the particle, momentum, and energy conservations, as well as Boltzmann's H-theorem[11, 13, 14].

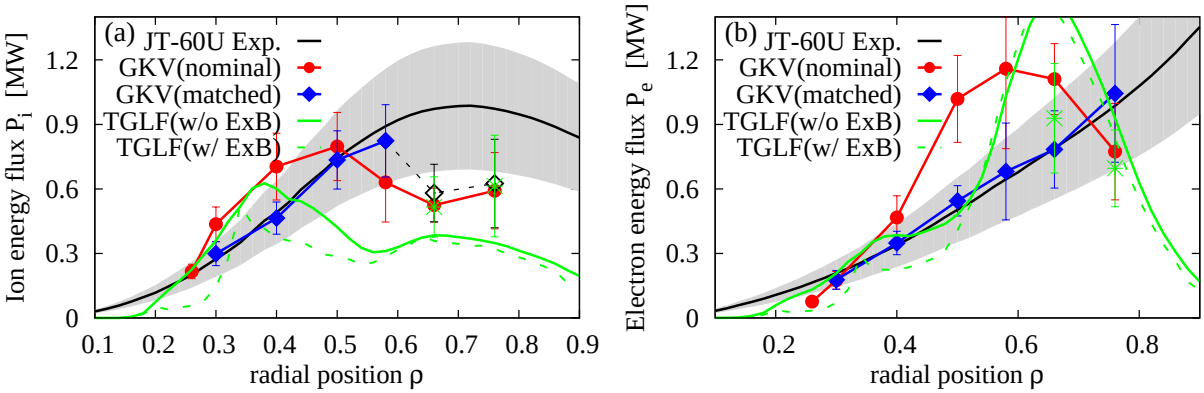

FIG. 1: Comparisons of (a)ion energy flux P_i, (b)electron energy flux P_e against the experimental results(incl. measurement errors shown by grey), where GKV results with nominal profile parameters and with modified $L_{T_\mathrm{i}}^{-1}$ and $L_{T_\mathrm{e}}^{-1}$ for the flux-matching are displayed. TGLF results with and without the mean-$E\times B$ shear are also plotted.

The electromagnetic fluctuations are determined by the Poisson-Ampère equations:

$$\left(k_\perp^2+\lambda_\mathrm{D}^{-2}\right)\delta\phi_{\boldsymbol{k}_\perp} = 4\pi\sum_\mathrm{s} e_\mathrm{s}\int d\boldsymbol{v}\, J_{0\mathrm{s}}(k_\perp v_\perp/\Omega_\mathrm{s})\,\delta g_{\mathrm{s}\boldsymbol{k}_\perp}\ , \tag{3}$$

$$k_\perp^2\,\delta A_{\parallel\boldsymbol{k}_\perp} = \frac{4\pi}{c}\sum_\mathrm{s} e_\mathrm{s}\int d\boldsymbol{v}\, v_\parallel J_{0\mathrm{s}}(k_\perp v_\perp/\Omega_\mathrm{s})\,\delta g_{\mathrm{s}\boldsymbol{k}_\perp}\ , \tag{4}$$

where $\lambda_\mathrm{D}=(\sum_\mathrm{s} 4\pi n_\mathrm{s} e_\mathrm{s}^2/T_\mathrm{s})^{-1/2}$ is the Debye length. The charge neutrality in the background density n_s is described as $\sum_{\mathrm{s}\neq\mathrm{e}} f_{C\mathrm{s}}=1$, where $f_{C\mathrm{s}}\equiv Z_\mathrm{s} n_\mathrm{s}/n_\mathrm{e}$ means the charge-density fraction for ions with the charge number Z_s. The contribution of each species to the source terms in the right hand side of Eqs. (3) and (4) is proportional to $f_{C\mathrm{s}}$. In addition, the radial derivative of the above charge neutrality condition leads to another constraint for the background density gradient, i.e., $\sum_{\mathrm{s}\neq\mathrm{e}} f_{C\mathrm{s}} L_{n_\mathrm{s}}^{-1} = L_{n_\mathrm{e}}^{-1}$. More details of the calculation model are given in, e.g., Ref. [10]. By using the above gyrokinetic Vlasov and Poisson-Ampère equations, one can derive the entropy balance/transfer equation [e.g., see Refs. [14, 15]] which provides us with a good measure for the turbulence simulation accuracy and useful physical insights associated with the turbulence saturation mechanisms.

2.2 Flux-matching validation of turbulent transport simulations in tokamak experiments

In order to examine the prediction capability of the flux-tube gyrokinetic simulations, we have carried out quantitative comparisons of the ion and electron turbulent transport between the simulation results and experimental measurements in JT-60U tokamak[4]. An

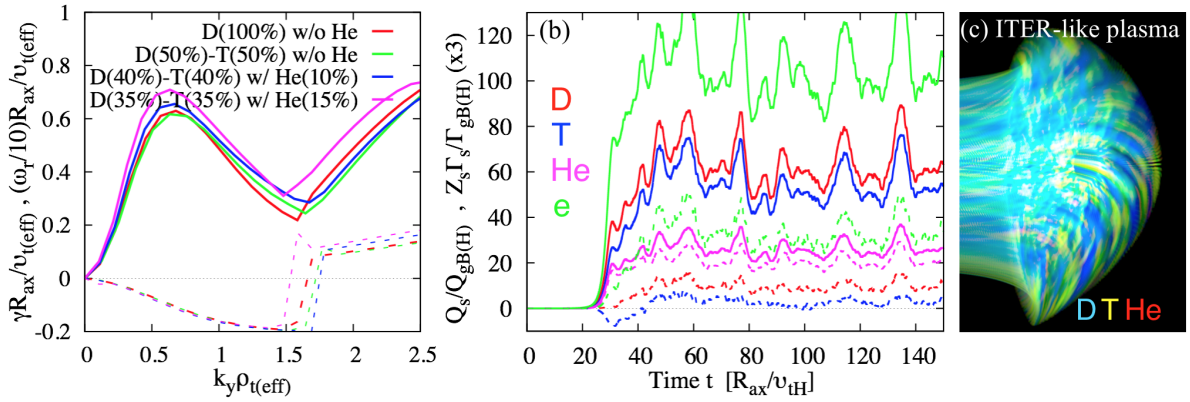

FIG. 2: (a)Normalized linear growth rate and mode frequency for the cases with D(30%)-T(30%)-He(10%), D(35%)-T(35%)-He(15%), D(50%)-T(50%) and D(100%). (b)Time evolution of turbulent energy(solid) and particle(dashed) fluxes in the D(40%)-T(40%)-He(10%) plasma. (c)Temperature fluctuations at $t = 80R_{ax}/v_{tH}$ of D(blue), T(yellow), and He(red) in the ITG-TEM turbulence.

L-mode plasma with sufficiently small ρ^* ($\sim 1/500$) is chosen for the validation in a local limit regime, where the mean radial electric field and its shearing effect are negligibly small. As shown in Figs. 1(a) and 1(b), nonlinear ITG and/or TEM simulations by GKV with the nominal experimental profile parameters successfully reproduce the radial profiles of the ion and electron energy fluxes which are comparable to the experimental values in the core region. The results with a gyrofluid-based transport model TGLF[16] also show similar energy transport levels for the ITG-dominated region of $\rho \leqslant 0.4$, but some differences are found in outer region with the TEM-dominated turbulence. Note that, since the L-mode plasma chosen here shows negligibly small radial electric fields, weak impact of the radial $E \times B$ shearing effect is confirmed in the TGLF cases. It is revealed that the zonal flow generation in the outer region($\rho > 0.58$) with TEM-dominated turbulence is much more significant than that in the core region($\rho \leqslant 0.58$). Then, about 40% under-prediction for the ion energy flux, which is the so-called transport shortfall, appears in the outer region.

By using a multiple flux matching technique for both the ion and electron energy fluxes, which is a generalization of the conventional flux matching with a single parameter of the ion temperature gradient, the prediction accuracy for the ion and electron temperature gradients is examined. Although the weak temperature-gradient dependence of TEM-driven turbulent transport and zonal flows in the the outer region prevents the flux matching, the temperature-gradient variations giving the matched energy fluxes in the core region(shown in blue lines in Figs. 1) are simultaneously identified for ions and electrons with the prediction error less than $\pm 30\%$.

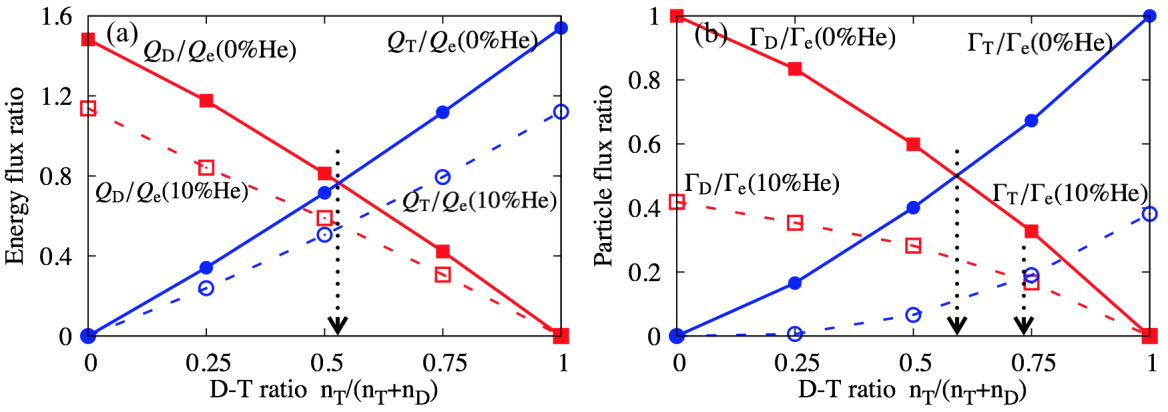

FIG. 3: D-T ratio dependencies of the mean (a)energy and (b)particle fluxes of D and T for 0%(solid) and 10%(dashed) He-ash accumulations, where the ion fluxes are normalized by the electron ones.

3 ITG-TEM driven turbulence simulations in ITER D-T-He plasma

3.1 Impacts of D-T ratio and He-ash accumulations on turbulent fluxes

In this section, we present multi-species turbulence simulations in ITG-TEM unstable plasma with realistic ITER-shape[10], where the impacts of D-T ratio and He-ash accumulations on turbulent fluxes are examined. Here, we assume the normalized temperature and density gradient lengths at $\rho = 0.5$ to be $R_{ax}/L_{T_i} = 6$(for all ions), $R_{ax}/L_{T_e} = 8$, and $R_{ax}/L_n = 2$, respectively. Also, $T_i = T_e = 5$keV, $n_e = 1.4 \times 10^{20}\mathrm{m}^{-3}$ are used, where the normalized electron-electron collisionality is $\nu^*_{ee} \sim 0.02$. The linear growth rate and mode frequency in the D-T-He plasma with 10% Helium-ash($n_{He}/n_e = 0.1$) are shown in Fig. 2(a), where the cases with D(35%)-T(35%)-He(15%), D(50%)-T(50%) and D(100%) are also plotted for comparisons. Note that the effective thermal speed $v_{t(eff)}$ and ion gyroradius $\rho_{t(eff)}$ are defined with the effective ion mass and charge numbers, i.e., $A_{eff} \equiv \sum_{s\neq e} f_{Cs} A_s$ and $Z_{eff} \equiv \sum_{s\neq e} f_{Cs} Z_s$. One can see a slight change of the normalized growth rate by the He-ash accumulation. The time evolution of turbulent energy and particle fluxes, i.e., Q_s and $Z_s\Gamma_s$, in the D(40%)-T(40%)-He(10%) plasma is shown in Fig. 2(b), where the gyro-Bohm units for hydrogen are used here. The ambipolar condition of $\Gamma_D + \Gamma_T + 2\Gamma_{He} = \Gamma_e$ is accurately satisfied. One finds different saturation levels, e.g., $Q_{He} < Q_T \sim Q_D \sim 0.5Q_e$ in the statistically steady state[Fig. 2(b)], where the snapshot of the temperature fluctuations in the real space is displayed in Fig. 2(c). Note also that the direction of the tritium particle transport flips after the saturation of the liner growth.

Figures 3(a) and 3(b) show the impact of the D-T fuel ratio $n_T/(n_T+n_D)$ on the mean turbulent energy and particle transport levels of D and T ($Q_{D,T}$ and $\Gamma_{D,T}$) in the cases

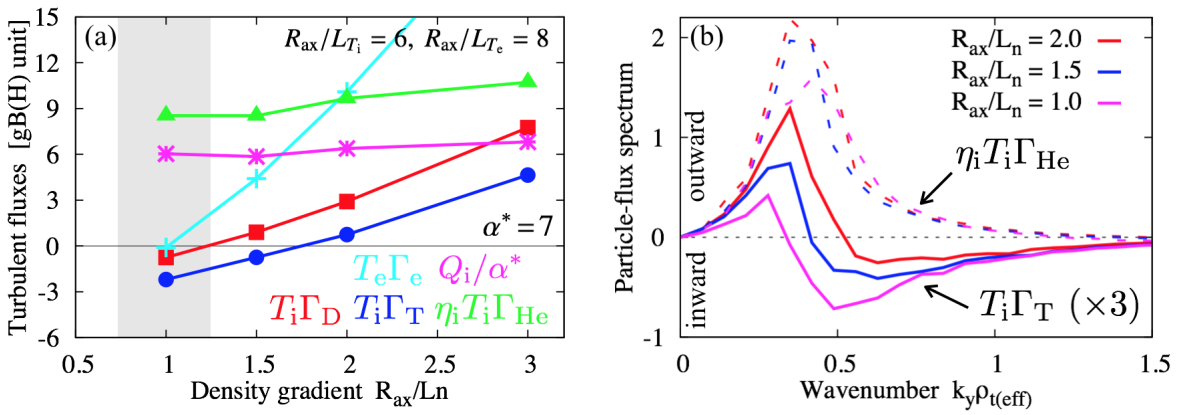

FIG. 4: (a)Density-gradient scan of turbulent particle and ion energy fluxes, where the steady burning condition with $\alpha^* = 7$ is satisfied in $R_{ax}/L_n \leq 1.27$(hatch region). (b)Wavenumber spectra of the tritium(solid) and He-ash(dashed) fluxes for the several density gradients.

with and without He-ash, where the ion fluxes are normalized by the electron ones (Q_e and Γ_e). Note that the both energy and particle fluxes for electrons are almost constant for all the cases, i.e., $Q_e/Q_{gB(H)} \simeq 110$ and $\Gamma_e/\Gamma_{gB(H)} \simeq 10$ ["gB(H)" denotes the hydrogen gyro-Bohm unit]. It is stressed that, for the case with He-ash, the additional transport channel of He-ash leads to the reduction in the energy and particle fluxes of D-T ions. One also finds that the overall tendency in the linear D-T ratio dependence of the energy fluxes is unchanged [Fig. 3(a)], e.g., $Q_D \simeq Q_T$ at the almost 50%-50% D-T ratio, regardless of the He-ash accumulations. On the other hand, in the D-T particle fluxes without He-ash, an imbalanced transport due to the nonlinear D-T ratio dependence is revealed [Fig. 3(b)], where $\Gamma_D \neq \Gamma_T$ even at 50%-50% D-T ratio. Moreover, the finite He-ash accumulations give rise to not only the reduction in the turbulent flux, but also stronger imbalance of the D-T particle transport. The detailed characteristics of the imbalanced particle transport depending on the background D-T ratio and He-ash can contribute to establishing more efficient D/T fueling and the density-profile controls in burning plasmas.

3.2 Gyrokinetic-simulation-based evaluation of steady burning condition

The present multi-ion species turbulence simulations with He-ash can provide the quantitative evaluation of the steady burning condition which can never be addressed by the single-ion-species approaches. For sustainable fusion reactions with the He-ash exhaust(outward flux) and fuel pinch(inward flux), a steady burning condition is given by $\Gamma_{He} > 0$, $\Gamma_{D,T} < 0$, and $(L_n/L_{T_i})T_i\Gamma_{He} > Q_i/\alpha^*$ (or equivalently $\tau_{He} < \alpha^*\tau_E$), where the mean D-T energy flux is denoted by Q_i, and $\alpha^* \sim 7-15$ is a constant depending on the divertor and wall conditions[5]. To this end, the density-gradient(R_{ax}/L_n) scans of the turbulent energy and particle transport are performed, where the case with D(40%),

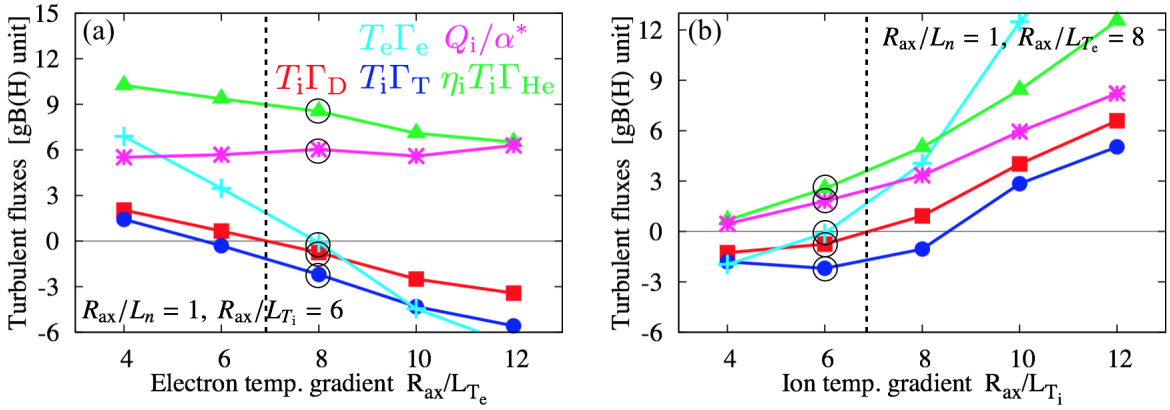

FIG. 5: Nonlinear scans of particle and energy fluxes on (a)electron-temperature, and (b)ion-temperature gradients, where the results encircled in black correspond to the profile regime, which satisfy the steady burning condition, shown in the hatch region of Fig. 4(a).

T(40%), and He(10%) ions is considered. As shown in Fig. 4(a), the density gradient dependence of Γ_D and Γ_T gives rise to a threshold of the inward D-T fluxes with $\Gamma_{D,T} \leqslant 0$ shown by the vertical dashed line, where it is expected that the inward pinch related to the off-diagonal contributions from $R_{ax}/L_{T_{i,e}}$ prevails over the outward diffusion from R_{ax}/L_n in the D-T particle fluxes. Moreover, the wavenumber spectra of $\eta_i T_i\Gamma_{He}$ and $T_i\Gamma_T$ shown in Fig. 4(b) indicate that, in contrast to the weak R_{ax}/L_n dependence of $\Gamma_{He} > 0$, the components of the inward tritium flux increase for the lower R_{ax}/L_n. Then, the profile regime of $R_{ax}/L_n \leq 1.2$(hatched region) that satisfies the above steady burning condition with $\alpha^* = 7$ is clearly identified. Note also that we see $\Gamma_e \simeq 0$ around $R_{ax}/L_n = 1$, which is necessary for the steady electron density profile.

In order to explore the other possible profile regime for the steady burning condition, which results from the off-diagonal contributions to the turbulent fluxes, R_{ax}/L_{T_e} and R_{ax}/L_{T_i} scans are performed as shown in Figs. 5(a) and 5(b), respectively, where $R_{ax}/L_n = 1$ is fixed, and the encircled symbols in each figure correspond to the previous one shown in the hatched region of Fig. 4(a). It is found that the larger R_{ax}/L_{T_e} tends to produce the inward particle fluxes for D, T, and electrons, while the opposite dependence appears for R_{ax}/L_{T_i}. Thus, another steady burning profile regime with steeper temperature gradients, but keeping $\Gamma_e \simeq 0$, is anticipated for larger R_{ax}/L_{T_e} and R_{ax}/L_{T_i}. Actually, it has been confirmed that the case with ($R_{ax}/L_n = 1$, $R_{ax}/L_{T_e} = 10$, $R_{ax}/L_{T_i} = 8$) also satisfies the steady burning condition, as well as ($R_{ax}/L_n = 1$, $R_{ax}/L_{T_e} = 8$, $R_{ax}/L_{T_i} = 6$).

4 Summary

In this study, the ITG-TEM driven turbulent transport in realistic ITER D-T-He plasma is investigated by means of multi-species electromagnetic gyrokinetic Vlasov simulations, where a good prediction capability has been confirmed against the JT-60U tokamak L-

mode experiment. It is found that the He-ash accumulation has stronger impacts on the turbulent particle fluxes, which lead to imbalanced D-T transport. Nonlinear scans with the various density and temperature gradient parameters reveal the off-diagonal contributions to the deuterium and tritium particle transport, and identify several profile regimes that satisfy the steady burning condition. These findings on the D-T ratio impact and on the profile dependence for the steady burning condition can contribute to deeper understanding of the multi-species transport processes in burning plasmas. More comprehensive scans for the steady burning condition in the parameter space with ($R_{\rm ax}/L_n$, $R_{\rm ax}/L_{T_{\rm i}}$, $R_{\rm ax}/L_{T_{\rm e}}$) including the radial dependence are useful for the integrated predictive simulations of kinetic profiles in ITER and DEMO.

This work is supported by the MEXT Japan, Grant No. 26820401, in part by the NIFS collaborative Research Programs, and in part by the MEXT grant for Post-K project:Development of innovative clean energy, Core design of fusion reactor, and in part by JT-60 collaboration programs. Numerical simulations were performed by Plasma Simulator at NIFS, HELIOS at IFERC-CSC, and K-computer at RIKEN-AICS.

References

[1] T. Görler *et al.*, Phys. Plasmas 21, 122307 (2014)

[2] D. Told *et al.*, Phys. Plasmas 20, 122312 (2013)

[3] C. Holland, Phys. Plasmas 23, 060901 (2016)

[4] M. Nakata *et al.*, Nucl. Fusion 56, 080016 (2016)

[5] C. Estrada-Mila *et al.*, Phys. Plasmas 12, 022305 (2005)

[6] C. Estrada-Mila *et al.*, Phys. Plasmas 13, 112303 (2006)

[7] C. Angioni *et al.*, Nucl. Fusion 49, 055013 (2009)

[8] C. Angioni, Phys. Plasmas 22, 102501 (2015)

[9] T. -H. Watanabe *et al.*, Nucl. Fusion 46, 24 (2006)

[10] M. Nakata *et al.*, Plasma Fusion Res. 9, 1403029 (2014)

[11] M. Nakata *et al.*, Comput. Phys. Commun. 197, 61 (2015)

[12] D. Reiter *et al.*, Nucl. Fusion 30 2141 (1990)

[13] M. Nunami *et al.*, Plasma Fusion. Res. 10, 1403058 (2015)

[14] H. Sugama *et al.*, Phys. Plasmas 16, 112502 (2009)

[15] M. Nakata *et al.*, Phys. Plasmas 19, 022303 (2012)

[16] G. M. Steabler *et al.*, Phys. Plasmas 14, 055909 (2007)